An *in situ* atlas of mitochondrial DNA in mammalian tissues reveals high content in stem/progenitor cells

Running head: An *in situ* hybridization assay for mtDNA

Jiayu Chen[1], Qizhi Zheng[1], Lauren B. Peiffer[1,2], Jessica L. Hicks[1], Michael C. Haffner[1,3], Avi Z. Rosenberg[1], Moshe Levi[4], Xiaoxin X. Wang[4], Busra Ozbek[1], Srinivasan Yegnasubramanian[3,5], Angelo M. De Marzo[1,3,5*]

[1]Department of Pathology, Johns Hopkins University School of Medicine, Baltimore, Maryland 21231, USA;

[2]Department of Molecular and Comparative Pathobiology, Johns Hopkins University School of Medicine, Baltimore, Maryland 21231, USA;

[3]Sidney Kimmel Comprehensive Cancer Center, Johns Hopkins University School of Medicine, Baltimore, Maryland 21231, USA;

[4]Department of Biochemistry and Molecular and Cellular Biology, Georgetown University, Washington DC 20057, USA;

[5]Departments of Urology and Oncology, Johns Hopkins University School of Medicine, Baltimore, Maryland 21231, USA.

*Correspondence: Angelo M. De Marzo, Department of Pathology, Johns Hopkins University School of Medicine, CRB-2/Room 144, 1550 Orleans Street, Baltimore, MD 21231, USA. E-mail: ademarz@jhmi.edu

ABSTRACT

Mitochondria regulate ATP production, metabolism and cell death. Alterations in mitochondrial DNA (mtDNA) sequence and copy number are implicated in aging and organ dysfunction in diverse inherited and sporadic diseases. Since most measurements of mtDNA use homogenates of complex tissues, little is known about cell type-specific mtDNA copy number heterogeneity in normal physiology, aging and disease. Thus, the precise cell types whose loss of mitochondrial activity and altered mtDNA copy number that result in organ dysfunction in aging and disease have often not been clarified. Here, we validated an *in situ* hybridization approach to generate a single cell resolution atlas of mtDNA content in mammalian tissues. In hierarchically organized self-renewing tissues, higher levels of mtDNA were observed in stem/proliferative compartments compared to differentiated compartments. Striking zonal patterns of mtDNA levels in the liver reflected the known oxygen tension gradient. In the kidney, proximal and distal tubules had markedly higher mtDNA levels compared to cells within glomeruli and collecting duct epithelial cells. Decreased mtDNA levels were visualized in renal tubules as a function of aging, which was prevented by calorie restriction. We provide a novel approach for quantifying species- and cell type-specific mtDNA copy number and dynamics in any normal or diseased tissue and can be used for monitoring the effects of interventions in animal and human studies.

INTRODUCTION

Mitochondria are critical for many cellular functions including ATP production, metabolism, macromolecular synthesis, calcium homeostasis, cell signaling and programmed cell death.[1] Mitochondria have their own genome (mitochondrial DNA or mtDNA), encoding 16 proteins involved in oxidative phosphorylation, 22 transfer RNAs, and 2 ribosomal RNAs required for mitochondrial ribosome function. Over the last few decades a large number of genetic diseases of mitochondrial function have been characterized that are caused by maternally inherited mutations in the mitochondrial genome, or by nuclear encoded genes whose products function in mitochondria.[1,2] These mutations often result in disorders of the nervous system (e.g. epilepsy, deafness, neuropathy, ataxia), skeletal muscle (e.g. weakness, ophthalmoplegia), and cardiac muscle (e.g. cardiomyopathy). Interestingly, a number of inherited diseases caused by mtDNA mutations, or mutations in nuclear genes whose products function in mitochondria, demonstrate organ-specific and cell type-specific phenotypes.[3]

Mitochondrial dysfunction can also be acquired in the absence of inherited mutations, and has been linked to declines of function with aging in several organ systems and to age-related cardiovascular and neurodegenerative diseases, as well as cancer.[4–7] Whether these age-related declines in mitochondrial function directly result from the known accumulation of somatic mtDNA mutations, or sub-genomic deletions with age, is still unclear.[6,8]

Mitochondrial function can be regulated through mitochondrial biogenesis, which is controlled in a cell-type and tissue-specific manner and is determined in part by regulating mtDNA copy number.[9] As such, there has been interest in measuring mtDNA copy number (independent of mtDNA mutations) in aging and diseased tissues.[10–16] In human studies, while there is general agreement that mtDNA copy number declines with age in peripheral blood

Page 3

mononuclear cells,[17–20] no consensus has been reached regarding mtDNA copy number changes with aging in non-blood related tissue types.[15] This is the case even in skeletal muscle, in which both overall cellular/organ function and mitochondrial function are well-known to decline with age. The discrepancies in the results from these studies do not appear to be explained simply by methodological differences.[15] Since widely employed strategies for measuring mtDNA levels are performed using solution-based methods after cellular disruption/homogenization of bulk tissues, the measurements necessarily reflect a composite of heterogeneous cell types. Therefore, it has been suggested that some of the discrepancies may be related to the fact that tissues are composed of multiple cell types, whose proportions can change in a variable manner with aging due to processes such as inflammation, regeneration, and fibrosis.[8] One method that has been used in attempts to circumvent the problem of heterogeneous cell types is to isolate specific cell populations (e.g. in the liver and CNS) by laser capture microdissection followed by quantitative PCR (qPCR) or genomic sequencing.[16,21] Yet, even using laser capture it can be very difficult to evaluate specific cell types or single cells across tissue samples. Therefore, an *in situ* method for mtDNA measurements would be advantageous. While prior studies have used *in situ* approaches to localize mtDNA in cells and tissues, these methods were used in limited applications, such as those regarding mtDNA replication and transcription, as well as to examine mtDNA levels in specific cell populations in a single tissue type or disease state.[22–33] In this study we developed a novel quantitative *in situ* assay to interrogate mtDNA at the single cell level in formalin fixed paraffin embedded (FFPE) or frozen archival tissue. By contrast to bulk methods, this *in situ* approach can be implemented using standard bright field microscopy facilitating rapid spatial determination of mtDNA content at single cell resolution in complex tissues.

MATERIALS AND METHODS

Cell Culture and Treatment

Prostate cancer cell lines CWR22Rv1 (CRL-2505), LNCaP (CRL-1740) and PC3 (CRL-1435) were obtained from American Type Culture Collection (ATCC, Manassas, VA). All cell lines were cultured in RPMI 1640 with L-glutamine media (Corning, Corning, NY) and 10% heat inactivated BenchMark™ Fetal Bovine Serum (FBS, Gemini Bio-Products, West Sacramento, CA). Cells were maintained in 75 cm^2 or 175 cm^2 TC flasks (Sarstedt, Germany) in a humidified incubator at 37°C with 5% CO_2. When reaching ~85% confluency, cells were passaged using TrypLE™ Express Enzyme without phenol red (Thermo Fisher, Waltham, MA). All cell lines were authenticated using Short Tandem Repeat (STR) profiling by the Genetic Resources Core Facility at The Johns Hopkins University School of Medicine.

To generate cells with different level of mtDNA, CWR22Rv1 and PC3 cells were cultured in RPMI 1640 with L-glutamine media (Corning) containing 2',3'-Dideoxycytidine (ddC, D5782, MilliporeSigma, Burlington, MA), 10% FBS, 1 mM Sodium Pyruvate (Thermofisher) and 50 µg/mL Uridine (MilliporeSigma). ddC containing media was replaced twice a week.

Cell Block Preparation

Formalin-fixed paraffin-embedded (FFPE) cell blocks were generated using the protocols described previously with the following modifications.[34] Cells were harvested by trypsinization as above, washed once with PBS, and resuspended in ~ 150 µL 10% neutral buffered formalin (NBF). The resuspended cells were transferred to a 0.5 mL microcentrifuge tube with solidified 2% agarose prefilled in the tapered portion of the bottom, and spun down in a swinging bucket centrifuge at 1000 rpm for 5 min. The resulting supernatant was removed, and fresh 10% NBF

was added without disturbing the pellet. The microcentrifuge tube was spun at 1500 rpm for 5 min, and the resulting cell plug was fixed in formalin for 48 hours at room temperature by submerging the microcentrifuge tube into a 15 mL conical tube containing 10% NBF. After fixation, the microcentrifuge tubes were transferred to a new 15 mL conical tube with PBS and stored at 4°C prior to processing and embedding in paraffin blocks.

Human Prostate, Small Intestine, Liver, Kidney and Tissues

Prostate tissues were obtained from radical prostatectomies for prostate cancer. Human duodenum (small intestine) was obtained as frozen tissue samples of grossly normal duodenum from patients undergoing pancreatoduodenectomy for pancreatic cancer. Human liver and kidney tissues were obtained from samples of patients undergoing autopsy for metastatic prostate cancer. This study was approved by the Johns Hopkins institutional internal review board.

Normal Mouse Tissues

Experimentally unmanipulated wild type normal (FVB/N mice (derived from FVB-Tg (ARR2/Pbsn-MYC)7Key/Nci) were conventionally housed according to protocols approved by the Animal Care and Use Committee at Johns Hopkins University. Animals (2-3 months, n = 3 for each sex) were euthanized, necropsied dissected as previously described,[35] and tissues were fixed in 10% NBF or Formical-2000 for bone tissues samples (StatLab) for 48 hours and processed into FFPE blocks as above.

Mouse Aging and Calorie Restriction Study

Male mice (C57BL/6, NIA) were housed and maintained on a 12 hour light-dark cycle, at a constant temperature (22 ± 2°C) and relative humidity (55 ± 15%) and treated as described.[36] Mice were randomly divided into the following groups: Group 1 - control young (6 months, n=3); Group 2 - control aging (24 months, n=3), Group 3 - aging with calorie restriction (24 months, n=3). Tap water was available ad libitum and rodent diets were available *ad libitum* for groups 1 and 2. For group 3, mice were calorie restricted (40% calorie reduction) from 14 weeks of age. Immediately following euthanasia, the kidneys were harvested and processed for FFPE.

mtDNA ISH Assay

Chromogenic *in situ* hybridization (CISH) of mtDNA on FFPE prostate tissues and FFPE cell blocks was performed manually following the instructions from the manufacturer (Advanced Cell Diagnostics, or ACD, Newark, CA) using RNAscope® 2.5 HD Detection Kit (BROWN) with the following modifications.[37] Slides were baked at 60°C for 30 min, deparaffinized in xylene 3 times for a total of 20 min, and in 100% ethanol (EtOH) 2 times for 4 min. Slides were then incubated in Pretreatment I solution (H_2O_2) for 10 min at room temperature, and steamed in Pretreatment II solution for 18 min. Slides were dipped in deionized water (diH$_2$O) with 0.1% Tween 20 (Source) once, and incubated in Protease Plus solution at 40°C as Pretreatment III. The protease digestion time depended on the sample types and species from 10 min (human cell blocks) to 20 or 30 min for the human and mouse tissues. Slides were incubated in Hs-MT-COX1-sense probe (Cat No. 478051) or Mm-Mt-Cox1-sense probe (Cat No. 530891), depending on the species, for 2 hours followed by the standard amplification steps as instructed

by the manufacturer. Probes were diluted in RNAscope® Probe Diluent and used at 1:200 for FFPE human prostate tissues and cell blocks, and 1:300 for FFPE mouse tissues.

Whole slides were scanned using a Roche-Ventana DP200 (Roche) or a Hamamatsu Nanozoomer XR whole slide scanner (Hamamatsu Photonics, Japan), and uploaded to Concentriq® (Proscia, Philadelphia PA) for whole slide image viewing and micrograph documentation.

For HALO image analysis, the Hs-MT-COX1-sense probe was used at 1:200 dilution, and visualized by alcohol-soluble ImmPACT® AEC Peroxidase (HRP) Substrate (SK-4205, Vector Laboratory, Burlingame, CA), mounted in aqueous media (VectaMount® AQ, H-5501, Vector Laboratory). After whole slide scanning, coverslips were removed by soaking in diH$_2$O and residual mounting media was washed away with fresh diH$_2$O. The polymerized AEC chromogenic situ signals were then removed by washing in 100% ethanol, and these "hematoxylin-only" slides were mounted in Cytoseal 60 (8310-16, Thermo Fisher) and scanned again. Under these conditions, hematoxylin stains the entire cell including the cytoplasm. The ratio of the area of AEC-positive signals to total cellular area was used as the area-fraction of mtDNA signals.

ISH Validation

DNase and RNase pretreatments were performed using the manufacturer's suggested protocol (ACD) with the following modifications. For DNase pretreatment, after steaming in Pretreatment II, the slides were treated with 100 µL DNase reaction buffer containing 10 µL DNase I Reaction Buffer (10X), 1 µL (2 units) DNAse I (M0303S, New England BioLabs,

Ipswich, MA), and 89 µL nuclease-free H_2O. The slides were then incubated at 37°C for 10 min, washed in diH_2O for 3 times, followed by *in situ* Pretreatment III. Similarly, for RNase pretreatment, the slides were immersed in 50 µg/mL RNase A (EN0531, ThermoFisher) diluted in 0.01 M Tris-HCl buffer, incubated at 37°C for 30 min, washed extensively in phosphate buffered saline with Tween-20 (PBST, P3563, MilliporeSigma) followed by *in situ* Pretreatment II. Human MT-COX1-sense probe was used at 1:50 dilution. Xenografts of human PC3 and VCaP prostate cancer cell lines were performed as described previously.[38] Detection of mtDNA on mouse xenograft slides was performed using the CISH-DAB protocol as mentioned above. Both Mouse MT-COX1-sense probe and human MT-COX1-sense probe were used at 1:50 dilution.

Fluorescence *in situ* hybridization (FISH) of mtDNA on FFPE tissues was conducted manually according to the manufacturer's protocols using RNAscope® Multiplex Fluorescent Kit v2 (ACD).[37] Pretreatment and probe hybridization procedures remained the same as the one mentioned above for standard mtDNA CISH. During the signal amplification and development process, Opal™ Dyes (NEL741E001KT, NEL744E001KT and NEL744E001KT, PerkinElmer, Waltham, MA) were used at 1:3500 in the TSA buffer provided in the RNAscope® Multiplex Fluorescent Kit v2 for each probe. The slides were counterstained with DAPI, mounted in ProLong™ Gold Antifade Mountant (Thermo Fisher) and coverslipped.

Cultured adherent cells were prepared for RNAscope® *in situ* hybridization using the manufacturer's instructions with following modifications. CWR22Rv1 and PC3 cells were seeded on Nunc™ Lab-Tek™ II CC2™ Chamber Slides (Thermo Fisher) at ~ 30,000 cells/cm^2 two days before fixation. Cells were fixed for 30 min in 10% NBF, treated with H_2O_2, steamed in

Pretreatment II solution for 5 min, and incubated in Protease III diluted 1:15 in PBS before proceeding to probe hybridization.

Localization of the mtDNA *in situ* signal was validated using a multiplex assay consisting of FISH for mtDNA and immunofluorescence for a mitochondrial protein MRPL12.[39,40] Briefly, LNCaP cells grown on chamber slides were fixed in formalin and mtDNA FISH was performed using the same protocol as for FFPE tissues. The slides were incubated in MRPL12 primary antibody (HPA022853, MilliporeSigma) at 1:200 dilution in Antibody Dilution Buffer (ADB250, Roche, Switzerland) for 45 min at RT. Alexa Fluor 568 Goat anti-Rabbit IgG (H+L) antibody (A-11036, Thermo Fisher) was used as secondary antibody at 1:300 dilution in PBS for 45 minutes at room temperature. The slides were counterstained, mounted, and coverslipped in the same fashion as mentioned above for FISH. Confocal fluorescent images were taken using a Zeiss AxioObserver inverted microscope with LSM700 confocal module (Carl Zeiss, Germany).

Immunohistochemistry

Chromogenic immunohistochemistry was performed mainly using the automated Ventana Discovery ULTRA (Roche). The slides were steamed for 32 min in CC1 buffer (950-124, Roche) and incubated in the corresponding primary antibody at room temperature for 36 min. Anti-MTCO1 antibody was used at 1:8000 dilution (ab14705, abcam, Cambridge, MA) and Anti-COX IV antibody was used at 1:8000 dilution (3E11, 4850, Cell Signaling, Danvers, MA) as primary antibodies. The slides were developed using Discovery HQ HRP hapten-linked multimer detection kit (Roche).

Quantitative PCR

Total DNA from cell lines was extracted using the DNeasy Blood & Tissue Kit (Qiagen, Germany). Quantitative PCR was performed using TaqMan™ Universal Master Mix II, no UNG (Catalog # 4440043) and TaqMan® Gene Expression Assays (Thermo Fisher) on a CFX Connect™ or a CFX96™ Real-Time PCR Detection System (BioRad, Hercules, CA). The cycling conditions were: 95°C for 10 min, 40 cycles of 95°C for 15 seconds, 60°C for 1 min, followed by melt curve analysis. The quantity of each amplified product was calculated using a standard curve of genomic DNA from peripheral blood leukocytes from a healthy donor (Catalog #: D1234148, Lot #: C210220, Biochain, Newark, CA). To calculate relative mtDNA copy number, MT-CO1 and MT-ND1 genes were used as specific mitochondrial targets, and the beta globin locus transcript 3 (BGLT3) and complement 2 (C2) genes were selected to be the endogenous controls. Taqman® Assays were purchased from Thermo Fishers. Information was as following: *MT-CO1*, Assay ID Hs02596864_g1, Catalog # 4331182; *MT-ND1*; *BGLT3*, Assay ID Hs01629437_s1, Catalog # 4331182; and *C2*, Assay ID Hs03599683_cn, Catalog # 4400291. All qPCR reactions were performed in triplicate.

RESULTS

Development and Validation of an in situ mtDNA Copy Number Assay

Transcription of the circular mtDNA proceeds in both directions. Therefore, when targeting mtDNA by *in situ* hybridization, it is possible that probes will hybridize to either RNA or DNA, resulting in ambiguity in signal interpretation. However, most light strand transcripts are rapidly degraded, including those anti-sense to the *MT-CO1* gene.[41,42] Thus, to minimize the

potential of hybridization to mitochondrial RNA (mtRNA), we designed an ACD probe set targeting the antisense region of the *MT-CO1* gene (probe set referred to as Sense-MT-CO1-A). **Figure 1A** shows the results of chromogenic *in situ* hybridization (DNAscope CISH) using this probe set, in which highly intense DAB signals localize in a punctate distribution within the cytoplasm of an FFPE sample of human prostate cancer. Pre-treatment of slides with DNase I, but not with RNase A, abolished the signal, confirming specificity for DNA (**Figure 1**). To further validate the assay specificity, we treated prostate cancer cells (CWR22Rv1 and PC3) with 2′,3′-Dideoxycytidine (ddC) to reduce global mtDNA levels.[43] The nucleotide derivative of ddC, ddCTP, can interact with and inhibit the activity of DNA polymerase gamma (pol γ), which is the only DNA polymerase in the mitochondria, and thus inhibit mtDNA replication.[43] **Figure 2** shows the results in which there was a ddC dose responsive reduction in hybridization signals in both cell lines.

To determine if this *in situ* assay would provide a truly quantitative assessment of the mtDNA content, we correlated the mtDNA levels measured by CISH with mtDNA measurements by quantitative PCR (qPCR).[44,45] As standards, we treated PC3 and CWR22Rv1 cells with a single dose of ddC for varying times. At each time point, cells were harvested and split into two portions. The first was prepared for formalin fixation and paraffin embedding (FFPE), and the second was used for qPCR using the *MT-CO1* mtDNA locus normalized to the nuclear DNA gene, *BGLT3*. In a second qPCR reaction we used the mtDNA encoded *MT-ND1* gene that was normalized to a different nuclear gene (*C2)*. **Figure 3A** shows a stepwise reduction in the ratio of mtDNA to nuclear DNA for each primer/probe set used for qPCR after treating cells for increasing times with ddC. The ratios of mtDNA/nuclear DNA content from these two sets of primer pairs were highly correlated (**Figure 3B**). **Figure 4A** shows a corresponding stepwise decrease in mtDNA *in situ* signals in relation to duration of drug treatment. While both cell lines

showed sharp reductions in mtDNA by both methods, in PC3 cells treated for 9 days the mtDNA signals were largely undetectable by CISH (**Figure 4A**) and extremely low by qPCR (**Figure 3**). For image analysis, we performed CISH using the alcohol soluble chromogenic substrate, AEC (**Figure 4B**). After hybridization and slide scanning, the chromagen (AEC) was dissolved in EtOH and the slides were re-scanned using the hematoxylin signals only (**Figure 4B, upper and lower right**). The ratio of mtDNA area to total cellular area was determined using Halo™. There was a strong positive correlation between real-time qPCR and the area-fraction of mtDNA signals by image analysis (**Figure 4C**).

When mtDNA is depleted, the mtDNA encoded mRNAs and proteins will also be greatly reduced.[27,46] As such, we found that the loss of mtDNA was accompanied by a marked reduction of the mtDNA encoded protein MT-CO1 in a time-dependent manner in response to ddC treatment, whereas the nuclear DNA-encoded COX-IV protein remained present as expected (**Supplementary Figure 1**).

The sequence identity between human mtDNA and mouse mtDNA in the targeted regions of the *MT-CO1* gene is 77.8%. A prior study using RNAscope technology to distinguish mouse and human gene expression at the RNA level showed that for probe sets with <85% homology the probes did not cross hybridize.[47] Therefore, we further tested the specificity of the hybridization using human cancer cells grown as xenografts in mice. Hybridization signals for the human *MT-CO1* probe set were observed exclusively in the human tumor cells but not in the mouse stromal cells (**Supplementary Figure 2**). Conversely, a probe set developed to the mouse *mt-Co1* gene showed signals only in the mouse stromal cells and not in the human cells (**Supplementary Figure 2**). This result is consistent with the high specificity of these DNAscope hybridization reactions.[37,47,48]

To verify whether the *in situ* signals were localized to mitochondria, we used a fluorescence approach for *in situ* hybridization combined with immunofluorescence against MRPL12, a well-known mitochondrial protein.[39,40,49] As visualized by confocal microscopy (**Supplementary Figure 3**), the punctate signals for mtDNA and MRPL12 protein showed prominent areas of overlap in the cytoplasm, consistent with mitochondrial localization.

mtDNA Copy Number Survey of Normal Tissues by in situ Hybridization

Cellular and tissue heterogeneity of mtDNA copy number is poorly explored. We applied mtDNA CISH to various tissues from mice and humans. As an example of marked tissue/cell type heterogeneity, **Figure 5** shows a cross section from the neck region of a mouse encompassing a range of normal tissues. Strong mtDNA signals were present in the basal layer (**Figure 5 C-D** and see below regarding stem cell compartments) of squamous epithelium in the esophagus, as well as in skeletal muscle, and glandular tissues including the tracheal epithelium, submucosal glands and thyroid (**Figure 5**). Very low hybridization signals were seen in tracheal cartilage (**Figure 5B**), consistent with its known lack of internal blood vessels and low mitochondrial mass. Brown adipose tissue (**Figure 5 E-F**) showed very high levels of mtDNA signals, in line with the well-known high levels of mitochondria in this tissue, compared to white adipose tissue.[50–52] Salivary glands showed a pattern in which the ducts showed higher mtDNA signals compared to the acini (not shown).

As expected, we found relatively high levels of mtDNA hybridization signals in cardiac muscle tissue, commensurate with their high energy demands and known high mitochondrial mass (not shown). In the pancreas, the islets showed more mtDNA signals than the exocrine acini (not shown). This corresponds to the observations of higher mitochondrial protein

expression in pancreatic islets versus acini.[53] In the urinary bladder, there were strikingly high levels of mtDNA signals in umbrella cells in female mice, as compared to the underlying intermediate or basal cells, which were higher than the detrusor muscle and other mesenchymal tissues (**Supplemental Figure 4**).

Adrenal Gland

The mouse adrenal showed marked differences in mtDNA signals by zone. In the cortex there appeared to be a slight gradation of signals, with somewhat stronger signals towards the capsule in the zona glomerulosa, and a tapering of signals in the zona fasciculata towards the medulla (**Figure 6**). Mice do not have a zona reticularis,[54] but in female mice the X-zone showed higher levels of mtDNA than the zona fasciculata. Strikingly, the adrenal medulla showed much lower mtDNA signals than the cortex **(Figure 6)**, in both males and females, which is consistent with prior results by qPCR.[55]

Kidney

In the mouse kidney we found robust signals in cortical tubular epithelial cells and strikingly low signal levels in cells within glomeruli (**Figure 7**). Distal convoluted tubular epithelium showed stronger signals than in proximal tubules. In collecting ducts, present in the cortex in medullary rays, and in the medulla, there were markedly reduced mtDNA hybridization signals compared to proximal and distal tubules. We found a highly similar pattern in human kidney tissues (not shown). As an additional control for hybridization efficiency in the different renal parenchymal compartments, we performed DNA *in situ* hybridization for telomeres using a

highly similar chromogenic approach.[34,56] We found similarly strong telomeric DNA signals in glomeruli as well as throughout the different renal tubules, supporting the likelihood that lower levels of mtDNA signals are not related to failure of probe penetration (not shown).

Liver

In the mouse liver there was a striking zonal distribution to mtDNA hybridization signals such that periportal hepatocytes (zone 1) showed the highest levels, with an apparent gradient of lower levels towards the hepatocytes surrounding the central veins (zone 3) (**Figure 8**). This result is consistent with a recent study by Brosch et al. who examined next generation DNA sequencing data for mtDNA after laser capture microdissection of different human liver zones.[21]

Self-renewing Tissues with Stem Cell Compartmentalization

Based on the findings above in the esophagus (**Figure 5 above**), we performed mtDNA CISH in other continuously self-renewing tissues containing hierarchical differentiation, starting with other stratified squamous epithelia. In each stratified squamous tissue examined, including mouse skin, cervix, vagina, oropharynx, and esophagus, the cells in the basal compartment showed higher mtDNA signals than cells toward the surface (**Supplemental Figure 5** shows cervix; other sites not shown). In mouse hair follicles, those that are in the anagen growth phase showed intense signals in the deepest regions with a gradation of signals towards the skin surface (**Supplemental Figure 6)**. Also, these anagen phase regions showed considerably higher mtDNA signals compared with those in telogen phase (**Supplemental Figure 6)**. This result agrees with previous studies showing higher mitochondrial activity by Mitotracker in

anagen cells than telogen cells.[57] In the gastrointestinal tract, the human (**Figure 9**) and mouse small intestine showed more mtDNA signals in the crypts, where the stem cells and transient amplifying/proliferative compartment cells are located, compared to the villus tips (**Figure 9**). A similar pattern was present in the colon of both mouse and human, and mouse stomach, where the stem/proliferative cells in the isthmus showed higher mtDNA signals than the surface or deeper glands (**Supplemental Figure 7).** We conclude that in each rapidly self-renewing tissue type that is organized using hierarchical differentiation, the stem cell/proliferative cell compartments contain higher mtDNA signals compared to the more differentiated cells.

Male Reproductive Tissues

In the prostatic epithelium, basal cells contained increased signals in general as compared to luminal cells (**Supplemental Figure 8**), and the epithelium showed overall higher signals than the stroma. The higher mtDNA content in the basal cell layer might be due to the fact that MYC is almost exclusively expressed in the basal cells,[58–60] and MYC has been shown to regulate mitochondrial biogenesis,[58] raising the question that mtDNA levels in some tissues are physiologically regulated by MYC (see Discussion). In the seminiferous tubules of the testis, we observed strong signals in germ cells adjacent to the basement membrane with an overall decrease in signals as cells differentiated towards mature sperm in the lumens (**Supplemental Figure 9**), which is consistent with prior studies,[61,62] In the epididymis, there were more mtDNA signals in the tail epithelium as compared with epithelium in the head (**Supplemental Figure 9**).

Female Reproductive and Urinary Tissues

The epithelium in mouse fallopian tube and uterus had strong mtDNA *in situ* signals (**Supplemental Figure 10**). In the mouse ovary, in regions containing follicles, there were very strong signals in the granulosa cells directly surrounding the oocytes, with many, albeit less numerous, signals in the oocyte cytoplasm. In addition, immature corpora lutea showed higher mtDNA signals compared to the mature corpora lutea (**Supplemental Figure 10**). Mouse epithelial cells in the endometrium showed clearly higher mtDNA signals as compared with endometrial stroma (**Supplemental Figure 10**).

Central Nervous System

In the central nervous system, neuronal cell bodies generally contained much stronger signals than surrounding glial cells and white matter. **Supplemental Figure 11** illustrates this in the mouse cerebellum which shows strong signals in Purkinje cell neuronal cell bodies and in neuronal cell bodies within a deep cerebellar nucleus.

Aging Kidney and Calorie Restriction

Kidney function is known to decrease gradually with increasing age in mammals, which has been associated with a gradual decline in mitochondrial function.[63–65] A recent study found that the ratio of mtDNA to nuclear DNA decreased in the aging mouse kidney.[36] Further, this reduction was prevented by calorie restriction, which is consistent with the finding that calorie restriction can prevent age-related declines in mitochondrial biogenesis and function in the

kidney.[36] However, which compartments in the kidney are most affected by these changes were not explored. Therefore, we examined the effects of aging and calorie restriction on mouse mtDNA levels in the kidney using our *in situ* assay. Mice were either fed *ad libitum* or treated with calorie restriction and then aged to 24 months. Tissue sections from the mouse kidneys were hybridized for mtDNA. After whole slide scanning and blinding of the slides, a visual microscopic review was conducted by two separate observers. Using this blind review, each observer separated the mice into two groups. One group of 3 mice contained variably lower levels of mtDNA in all tubule compartments by visual estimate (**Figure 10** shows cortical tubules) and was composed of the aging mice fed *ad libitum*. Although a general reduction in mtDNA signals was present throughout the kidney, in some of the cortical tubules there were markedly reduced signals, and this was only seen in the *ad libitum* fed older mice (**Figure 10)**. The other group (N=6), which did not show these isolated areas of markedly reduced mtDNA signals, consisted of a combination of younger mice fed *ad libitum* and aged calorie-restricted mice; these two treatment groups were visually indistinguishable.

DISCUSSION

There is no gold standard for measuring cell-type heterogeneity in mtDNA copy number in tissue samples. We present a novel approach that is widely applicable, straight-forward to implement and can be used either qualitatively or quantitatively. A key finding using this approach, that was not previously appreciated, is that in tissues organized into self-renewing hierarchical stem cell driven differentiation systems,[66] cells within stem cell/proliferative compartments contain higher mtDNA levels compared to their more differentiated progeny. This finding raises a number of important questions. The first involves our understanding of mtDNA

replication. While it is known that mtDNA replication is uncoupled from cell cycle progression (e.g. nuclear DNA replication) in some mitotic and post mitotic cells,[67,68] a number of groups have shown mtDNA replication appears to be synchronized during the cell cycle in cell culture systems.[31–33,69] Thus, the findings to date are somewhat contradictory. Future studies using an *in situ* approach, coupled with the ability to visualize newly synthesized mtDNA and nuclear DNA in intact tissues, can help clarify this question.

Another question is how mtDNA levels are regulated in the self-renewing tissues described herein. Key regulators of mtDNA replication are peroxisome proliferator activated receptor coactivator 1 alpha (PGC1-α; encoded by *PPARGC1A*) and peroxisome proliferator activated receptor coactivator 1 beta (PGC-1β; encoded by *PPARGC1B*). Further, MYC has been shown to drive mtDNA replication and mitochondrial biogenesis.[58] Interestingly, in the intestine[70] and squamous epithelia,[71] MYC levels are highest in regions that clearly overlap with those we have found have the highest mtDNA levels, raising the possibility that physiological regulation of mtDNA during tissue renewal in many stem cell compartments is governed, at least in part, by MYC. In fact, in mice with targeted disruption of *Myc* in the intestine, Myc-deficient crypts are lost, and Myc is required for successful progression through the cell cycle.[70] It is possible, therefore, that one mechanism by which Myc functions in the intestine is to induce mtDNA replication and mitochondrial biogenesis. Future studies are needed to address the question regarding the regulation of mtDNA levels in normal self-renewing tissues by MYC. Other genes related to mitochondrial function also appear to be required for intestinal stem cell maintenance since mice with targeted disruption of the key mitochondrial protein chaperone, hsp60, show loss of stem cells and proliferative capacity.[72] Another question is why prior studies have not shown the stark differences we observed in stem/proliferative compartments in mtDNA levels.[72] To gain some insight into this we are currently performing IHC against a number of

mitochondrial enzymes and *in situ* hybridization for mtRNAs. Our preliminary findings in the human intestine is that that mitochondrial protein markers do not correlate with mtDNA levels, but that 12S rRNA (*MT-RNR1*) does.

In the kidney of young healthy mice and humans, striking differences in mtDNA levels within different renal epithelial compartments were observed. First, we verified much lower levels of mtDNA in virtually all cell types present within the glomeruli.[28] Interestingly, distal tubules showed higher mtDNA levels than proximal, and collecting ducts showed markedly lower levels than proximal or distal tubules. Prior studies have shown a reduction in mtDNA to nuclear DNA by PCR based assays in aging mouse kidney tissues, and this could be prevented by calorie restriction,[36] treatment with a dual agonist of the farnesoid X receptor (FXR) and the G protein-coupled receptor TGR4, INT-767,[36] or the estrogen related receptors ERRα, ERRβ, and ERRγ.[65] Consistent with this, in the present study we found that the marked reduction in mtDNA levels was visualized in a number of tubule compartments and was prevented by calorie restriction. The current *in situ* approach will be useful to determine whether similar changes are seen in the human kidney with aging and how mtDNA levels are altered in different renal pathologies.

Another interesting finding was the remarkable zonal differences in mtDNA numbers in hepatocytes that is quite consistent with the known oxygen gradient, as well as, a recent study using NGS from laser capture microdissected zones of the liver.[21]

The ability to routinely interrogate mtDNA levels at the cellular level in the context of normal and abnormal spatial organization of cell types should greatly facilitate approaches to deciphering changes that occur in mtDNA in a number of disease states, including different cancers,[73] their precursor lesions and a large spectrum of non-neoplastic clinical disorders.

These include inherited autosomal and mtDNA syndromes that affect mtDNA copy number[74] that involve a number of organ systems and cell types (e.g. involving skeletal and cardiac muscle, neurons in Parkinson's disease and other neurodegenerative disorders, hepatocytes in liver, etc.). We submit that *in situ* studies of the involved tissues using the current approach can facilitate novel insights into disease pathogenesis and response to therapies.

In summary, we present a novel, quantitative and straightforward approach to mtDNA level measurements in tissue samples. This approach provides the first widely available opportunity to test changes that occur in mtDNA copy number in specific cell types, while retaining spatial information. The current study uncovered evidence of increased mtDNA copy number in stem/proliferative compartments throughout the body and serves as an initial phase towards the completion of a comprehensive cellular atlas of mtDNA copy number across tissues, and changes in such cell types in aging and disease. It should complement approaches using genomic methods, such as those using single cell RNA-seq and ATAC-Seq in which several large-scale efforts are underway. It can also complement other *in situ* approaches such as spatial transcriptomics, highplex IHC and *in situ* hybridization and prove useful in studies related to the effects of genotype, environmental exposures, and interventions (e.g. dietary or exercise) in model systems and humans.

ACKNOWLEDGEMENTS

REFERENCES

1. Gorman GS, Chinnery PF, DiMauro S, Hirano M, Koga Y, McFarland R, Suomalainen A, Thorburn DR, Zeviani M, Turnbull DM: Mitochondrial diseases. Nat Rev Dis Primers [Internet] 2016, 2:16080. Available from: http://dx.doi.org/10.1038/nrdp.2016.80

2. Taylor RW, Turnbull DM: Mitochondrial DNA mutations in human disease. Nat Rev Genet [Internet] 2005, 6:389–402. Available from: http://dx.doi.org/10.1038/nrg1606

3. Meyer JN, Hartman JH, Mello DF: Mitochondrial Toxicity. Toxicol Sci [Internet] 2018, 162:15–23. Available from: http://dx.doi.org/10.1093/toxsci/kfy008

4. Larsson N-G: Somatic mitochondrial DNA mutations in mammalian aging. Annu Rev Biochem [Internet] 2010, 79:683–706. Available from: http://dx.doi.org/10.1146/annurev-biochem-060408-093701

5. Ashar FN, Moes A, Moore AZ, Grove ML, Chaves PHM, Coresh J, Newman AB, Matteini AM, Bandeen-Roche K, Boerwinkle E, Walston JD, Arking DE: Association of mitochondrial DNA levels with frailty and all-cause mortality. J Mol Med [Internet] 2015, 93:177–186. Available from: http://dx.doi.org/10.1007/s00109-014-1233-3

6. Sun N, Youle RJ, Finkel T: The Mitochondrial Basis of Aging. Mol Cell [Internet] 2016, 61:654–666. Available from: http://dx.doi.org/10.1016/j.molcel.2016.01.028

7. Ashar FN, Zhang Y, Longchamps RJ, Lane J, Moes A, Grove ML, Mychaleckyj JC, Taylor KD, Coresh J, Rotter JI, Boerwinkle E, Pankratz N, Guallar E, Arking DE: Association of Mitochondrial DNA Copy Number With Cardiovascular Disease. JAMA Cardiol [Internet] 2017, 2:1247–1255. Available from: http://dx.doi.org/10.1001/jamacardio.2017.3683

8. Kauppila TES, Kauppila JHK, Larsson N-G: Mammalian Mitochondria and Aging: An Update. Cell Metab [Internet] 2017, 25:57–71. Available from: http://dx.doi.org/10.1016/j.cmet.2016.09.017

9. Clay Montier LL, Deng JJ, Bai Y: Number matters: control of mammalian mitochondrial DNA copy number. J Genet Genomics [Internet] 2009, 36:125–131. Available from: http://dx.doi.org/10.1016/S1673-8527(08)60099-5

10. Barazzoni R, Short KR, Nair KS: Effects of Aging on Mitochondrial DNA Copy Number and Cytochromec Oxidase Gene Expression in Rat Skeletal Muscle, Liver, and Heart. J Biol Chem [Internet] 2000, 275:3343–3347. Available from: http://www.jbc.org/content/275/5/3343.abstract

11. Cree LM, Patel SK, Pyle A, Lynn S, Turnbull DM, Chinnery PF, Walker M: Age-related decline in mitochondrial DNA copy number in isolated human pancreatic islets. Diabetologia [Internet] 2008, 51:1440–1443. Available from: http://dx.doi.org/10.1007/s00125-008-1054-4

12. Miller FJ, Rosenfeldt FL, Zhang C, Linnane AW, Nagley P: Precise determination of mitochondrial DNA copy number in human skeletal and cardiac muscle by a PCR-based assay: lack of change of copy number with age. Nucleic Acids Res [Internet] 2003, 31:e61. Available from: https://www.ncbi.nlm.nih.gov/pubmed/12771225

13. Kaaman M, Sparks LM, van Harmelen V, Smith SR, Sjölin E, Dahlman I, Arner P: Strong association between mitochondrial DNA copy number and lipogenesis in human white adipose tissue. Diabetologia [Internet], Springer, 2007, 50:2526–2533. Available from: http://dx.doi.org/10.1007/s00125-007-0818-6

14. Masuyama M, Iida R, Takatsuka H, Yasuda T, Matsuki T: Quantitative change in mitochondrial DNA content in various mouse tissues during aging. Biochim Biophys Acta [Internet] 2005, 1723:302–308. Available from: http://dx.doi.org/10.1016/j.bbagen.2005.03.001

15. Kazachkova N, Ramos A, Santos C, Lima M: Mitochondrial DNA damage patterns and aging: revising the evidences for humans and mice. Aging Dis [Internet] 2013, 4:337–350. Available from: http://dx.doi.org/10.14336/AD.2013.0400337

16. Dölle C, Flønes I, Nido GS, Miletic H, Osuagwu N, Kristoffersen S, Lilleng PK, Larsen JP, Tysnes O-B, Haugarvoll K, Bindoff LA, Tzoulis C: Defective mitochondrial DNA homeostasis in the substantia nigra in Parkinson disease. Nat Commun [Internet] 2016, 7:13548. Available from: http://dx.doi.org/10.1038/ncomms13548

17. Kim J-H, Kim HK, Ko J-H, Bang H, Lee D-C: The relationship between leukocyte mitochondrial DNA copy number and telomere length in community-dwelling elderly women. PLoS One [Internet] 2013, 8:e67227. Available from: http://dx.doi.org/10.1371/journal.pone.0067227

18. Mengel-From J, Thinggaard M, Dalgard C, Kyvik KO, Christensen K, Christiansen L: MITOCHONDRIAL DNA COPY NUMBER IN HUMAN PERIPHERAL BLOOD CELLS ASSOCIATE WITH AGE, SURVIVAL AND GENERAL HEALTH AMONG ELDERLY. GERONTOLOGIST, OXFORD UNIV PRESS INC JOURNALS DEPT, 2001 EVANS RD, CARY, NC 27513 USA, 2014, pp. 138–138.

19. Wachsmuth M, Hübner A, Li M, Madea B, Stoneking M: Age-Related and Heteroplasmy-Related Variation in Human mtDNA Copy Number. PLoS Genet [Internet]

2016, 12:e1005939. Available from: http://dx.doi.org/10.1371/journal.pgen.1005939

20. O'Hara R, Tedone E, Ludlow A, Huang E, Arosio B, Mari D, Shay JW: Quantitative mitochondrial DNA copy number determination using droplet digital PCR with single cell resolution: a focus on aging and cancer [Internet]. bioRxiv. 2019 [cited 2019 May 5], p. 579789. Available from: https://www.biorxiv.org/content/10.1101/579789v1.full

21. Brosch M, Kattler K, Herrmann A, von Schönfels W, Nordström K, Seehofer D, Damm G, Becker T, Zeissig S, Nehring S, Reichel F, Moser V, Thangapandi RV, Stickel F, Baretton G, Röcken C, Muders M, Matz-Soja M, Krawczak M, Gasparoni G, Hartmann H, Dahl A, Schafmayer C, Walter J, Hampe J: Epigenomic map of human liver reveals principles of zonated morphogenic and metabolic control. Nat Commun [Internet] 2018, 9:4150. Available from: http://dx.doi.org/10.1038/s41467-018-06611-5

22. Mita S, Schmidt B, Schon EA, DiMauro S, Bonilla E: Detection of "deleted" mitochondrial genomes in cytochrome-c oxidase-deficient muscle fibers of a patient with Kearns-Sayre syndrome. Proc Natl Acad Sci U S A [Internet] 1989, 86:9509–9513. Available from: http://dx.doi.org/10.1073/pnas.86.23.9509

23. Oldfors A, Larsson NG, Holme E, Tulinius M, Kadenbach B, Droste M: Mitochondrial DNA deletions and cytochrome c oxidase deficiency in muscle fibres. J Neurol Sci [Internet] 1992, 110:169–177. Available from: https://www.ncbi.nlm.nih.gov/pubmed/1324295

24. Müller-Höcker J, Seibel P, Schneiderbanger K, Kadenbach B: Different in situ hybridization patterns of mitochondrial DNA in cytochrome c oxidase-deficient extraocular muscle fibres in the elderly. Virchows Arch A Pathol Anat Histopathol [Internet] 1993, 422:7–15. Available from: https://www.ncbi.nlm.nih.gov/pubmed/7679851

25. Larsson NG, Wang J, Wilhelmsson H, Oldfors A, Rustin P, Lewandoski M, Barsh GS, Clayton DA: Mitochondrial transcription factor A is necessary for mtDNA maintenance and embryogenesis in mice. Nat Genet [Internet] 1998, 18:231–236. Available from: http://dx.doi.org/10.1038/ng0398-231

26. Rantanen A, Jansson M, Oldfors A, Larsson NG: Downregulation of Tfam and mtDNA copy number during mammalian spermatogenesis. Mamm Genome [Internet] 2001, 12:787–792. Available from: http://dx.doi.org/10.1007/s00335-001-2052-8

27. Janes MS, Hanson BJ, Hill DM, Buller GM, Agnew JY, Sherwood SW, Cox WG, Yamagata K, Capaldi RA: Rapid analysis of mitochondrial DNA depletion by fluorescence in situ hybridization and immunocytochemistry: potential strategies for HIV therapeutic monitoring. J Histochem Cytochem [Internet] 2004, 52:1011–1018. Available from: http://dx.doi.org/10.1369/jhc.3A6209.2004

28. Yamagata K, Muro K, Usui J, Hagiwara M, Kai H, Arakawa Y, Shimizu Y, Tomida C, Hirayama K, Kobayashi M, Koyama A: Mitochondrial DNA mutations in focal segmental glomerulosclerosis lesions. J Am Soc Nephrol [Internet] 2002, 13:1816–1823. Available from: https://www.ncbi.nlm.nih.gov/pubmed/12089377

29. Ashley N, Poulton J: Mitochondrial DNA is a direct target of anti-cancer anthracycline drugs. Biochem Biophys Res Commun [Internet] 2009, 378:450–455. Available from: http://dx.doi.org/10.1016/j.bbrc.2008.11.059

30. Kukat C, Wurm CA, Spåhr H, Falkenberg M, Larsson N-G, Jakobs S: Super-resolution microscopy reveals that mammalian mitochondrial nucleoids have a uniform size and frequently contain a single copy of mtDNA. Proc Natl Acad Sci U S A [Internet] 2011,

108:13534–13539. Available from: http://dx.doi.org/10.1073/pnas.1109263108

31. Chatre L, Ricchetti M: Large heterogeneity of mitochondrial DNA transcription and initiation of replication exposed by single-cell imaging. J Cell Sci [Internet] 2013, 126:914–926. Available from: http://dx.doi.org/10.1242/jcs.114322

32. Chatre L, Ricchetti M: Prevalent coordination of mitochondrial DNA transcription and initiation of replication with the cell cycle. Nucleic Acids Res [Internet] 2013, 41:3068–3078. Available from: http://dx.doi.org/10.1093/nar/gkt015

33. Chatre L, Ricchetti M: mTRIP: An Imaging Tool to Investigate Mitochondrial DNA Dynamics in Physiology and Disease at the Single-Cell Resolution. In: Weissig V, Edeas M, editors. Mitochondrial Medicine: Volume I, Probing Mitochondrial Function [Internet], New York, NY, Springer New York, 2015, pp. 133–147. Available from: https://doi.org/10.1007/978-1-4939-2257-4_13

34. Holdhoff M, Guner G, Rodriguez FJ, Hicks JL, Zheng Q, Forman MS, Ye X, Grossman SA, Meeker AK, Heaphy CM, Eberhart CG, De Marzo AM, Arav-Boger R: Absence of Cytomegalovirus in Glioblastoma and Other High-grade Gliomas by Real-time PCR, Immunohistochemistry, and In Situ Hybridization. Clin Cancer Res [Internet] 2017, 23:3150–3157. Available from: http://dx.doi.org/10.1158/1078-0432.CCR-16-1490

35. Brayton C, McKerlie C, Brown S: Analysis of Phenotype. Transgenic Animal Technology: A Laboratory Handbook: Third Edition [Internet], Elsevier Inc., 2014 [cited 2019 Dec 17], pp. 431–487. Available from: https://jhu.pure.elsevier.com/en/publications/analysis-of-phenotype-3

36. Wang XX, Luo Y, Wang D, Adorini L, Pruzanski M, Dobrinskikh E, Levi M: A dual agonist of

farnesoid X receptor (FXR) and the G protein-coupled receptor TGR5, INT-767, reverses age-related kidney disease in mice. J Biol Chem [Internet] 2017, 292:12018–12024. Available from: http://dx.doi.org/10.1074/jbc.C117.794982

37. Wang F, Flanagan J, Su N, Wang L-C, Bui S, Nielson A, Wu X, Vo H-T, Ma X-J, Luo Y: RNAscope: a novel in situ RNA analysis platform for formalin-fixed, paraffin-embedded tissues. J Mol Diagn [Internet], Elsevier, 2012, 14:22–29. Available from: http://dx.doi.org/10.1016/j.jmoldx.2011.08.002

38. Haffner MC, Esopi DM, Chaux A, Gürel M, Ghosh S, Vaghasia AM, Tsai H, Kim K, Castagna N, Lam H, Hicks J, Wyhs N, Biswal Shinohara D, Hurley PJ, Simons BW, Schaeffer EM, Lotan TL, Isaacs WB, Netto GJ, De Marzo AM, Nelson WG, An SS, Yegnasubramanian S: AIM1 is an actin-binding protein that suppresses cell migration and micrometastatic dissemination. Nat Commun [Internet] 2017, 8:142. Available from: http://dx.doi.org/10.1038/s41467-017-00084-8

39. Marty L, Fort P: A delayed-early response nuclear gene encoding MRPL12, the mitochondrial homologue to the bacterial translational regulator L7/L12 protein. J Biol Chem [Internet] 1996, 271:11468–11476. Available from: http://dx.doi.org/10.1074/jbc.271.19.11468

40. Wang Z, Cotney J, Shadel GS: Human mitochondrial ribosomal protein MRPL12 interacts directly with mitochondrial RNA polymerase to modulate mitochondrial gene expression. J Biol Chem [Internet] 2007, 282:12610–12618. Available from: http://dx.doi.org/10.1074/jbc.M700461200

41. Borowski LS, Dziembowski A, Hejnowicz MS, Stepien PP, Szczesny RJ: Human

mitochondrial RNA decay mediated by PNPase-hSuv3 complex takes place in distinct foci. Nucleic Acids Res [Internet] 2013, 41:1223–1240. Available from: http://dx.doi.org/10.1093/nar/gks1130

42. Mercer TR, Neph S, Dinger ME, Crawford J, Smith MA, Shearwood A-MJ, Haugen E, Bracken CP, Rackham O, Stamatoyannopoulos JA, Filipovska A, Mattick JS: The human mitochondrial transcriptome. Cell [Internet] 2011, 146:645–658. Available from: http://dx.doi.org/10.1016/j.cell.2011.06.051

43. Nelson I, Hanna MG, Wood NW, Harding AE: Depletion of mitochondrial DNA by ddC in untransformed human cell lines. Somat Cell Mol Genet [Internet], Springer, 1997, 23:287–290. Available from: https://www.ncbi.nlm.nih.gov/pubmed/9542530

44. Schubert S, Heller S, Löffler B, Schäfer I, Seibel M, Villani G, Seibel P: Generation of Rho Zero Cells: Visualization and Quantification of the mtDNA Depletion Process. Int J Mol Sci [Internet] 2015, 16:9850–9865. Available from: http://dx.doi.org/10.3390/ijms16059850

45. Brown TA, Clayton DA: Release of replication termination controls mitochondrial DNA copy number after depletion with 2',3'-dideoxycytidine. Nucleic Acids Res [Internet] 2002, 30:2004–2010. Available from: https://www.ncbi.nlm.nih.gov/pubmed/11972339

46. Liyanage SU, Hurren R, Voisin V, Bridon G, Wang X, Xu C, MacLean N, Siriwardena TP, Gronda M, Yehudai D, Sriskanthadevan S, Avizonis D, Shamas-Din A, Minden MD, Bader GD, Laposa R, Schimmer AD: Leveraging increased cytoplasmic nucleoside kinase activity to target mtDNA and oxidative phosphorylation in AML. Blood [Internet] 2017, 129:2657–2666. Available from: http://dx.doi.org/10.1182/blood-2016-10-741207

47. Li N, Ye XK, He M-X, Zhang B, Anderson CM, Luo Y, Ma X-J, Gu Z, Park E:

Species-specific gene expression profiling of patient-derived xenograft tumors by the RNAscope® in situ hybridization assay. thepathologist.com [Internet]. Available from: https://thepathologist.com/fileadmin/issues/App_Notes/01916-app-note-ACD-supplied.pdf

48. Wang H, Su N, Wang L-C, Wu X, Bui S, Nielsen A, Vo H-T, Luo Y, Ma X-J: Quantitative ultrasensitive bright-field RNA in situ hybridization with RNAscope. Methods Mol Biol [Internet], Springer, 2014, 1211:201–212. Available from: http://dx.doi.org/10.1007/978-1-4939-1459-3_16

49. Antonicka H, Sasarman F, Nishimura T, Paupe V, Shoubridge EA: The mitochondrial RNA-binding protein GRSF1 localizes to RNA granules and is required for posttranscriptional mitochondrial gene expression. Cell Metab [Internet], Elsevier, 2013, 17:386–398. Available from: http://dx.doi.org/10.1016/j.cmet.2013.02.006

50. Cinti S: Transdifferentiation properties of adipocytes in the adipose organ. Am J Physiol Endocrinol Metab [Internet] 2009, 297:E977–E986. Available from: http://dx.doi.org/10.1152/ajpendo.00183.2009

51. Farmer SR: Brown fat and skeletal muscle: unlikely cousins? Cell [Internet] 2008, 134:726–727. Available from: http://dx.doi.org/10.1016/j.cell.2008.08.018

52. Christoph H. Saely, Kathrin Geiger, Heinz Drexel: Brown versus White Adipose Tissue: A Mini-Review. Gerontology [Internet] 2010, . Available from: https://www.karger.com/article/pdf/321319

53. Yamazawa T, Nakamura N, Sato M, Sato C: Secretory glands and microvascular systems imaged in aqueous solution by atmospheric scanning electron microscopy (ASEM). Microsc Res Tech [Internet] 2016, 79:1179–1187. Available from:

http://dx.doi.org/10.1002/jemt.22773

54. Maronpot R: Pathology of the Mouse - Adrenal Gland - Toxicologic Pathology [Internet].

    Toxicologic Pathology. [cited 2019 Nov 21], . Available from:

    https://focusontoxpath.com/pathology-of-the-mouse-adrenal-gland/

55. Neuhaus JFG, Baris OR, Kittelmann A, Becker K, Rothschild MA, Wiesner RJ:

    Catecholamine Metabolism Induces Mitochondrial DNA Deletions and Leads to Severe

    Adrenal Degeneration during Aging. Neuroendocrinology [Internet] 2017, 104:72–84.

    Available from: http://dx.doi.org/10.1159/000444680

56. Ertunc O, Zheng Q, Smearman E, Hicks J, Brosnan-Cashman J, Jones T, Trabzonlu L,

    Heaphy C, Meeker A, De Marzo A: A Chromogenic In Situ Hybridization (CISH) Technique

    for Assessing Telomeric DNA Length in Formalin-Fixed Tissue Sections [Internet].

    Laboratory Investigation., 75 Varick St, 9th Flr, New York, Ny 10013-1917 USA, Nature

    Publishing Group, 2019, . Available from:

    http://apps.webofknowledge.com/full_record.do?product=WOS&search_mode=AdvancedS

    earch&qid=4&SID=7ATKVhbtvdj1LpXTM7t&page=1&doc=3

57. Tang Y, Luo B, Deng Z, Wang B, Liu F, Li J, Shi W, Xie H, Hu X, Li J: Mitochondrial aerobic

    respiration is activated during hair follicle stem cell differentiation, and its dysfunction

    retards hair regeneration. PeerJ [Internet] 2016, 4:e1821. Available from:

    http://dx.doi.org/10.7717/peerj.1821

58. Li F, Wang Y, Zeller KI, Potter JJ, Wonsey DR, O'Donnell KA, Kim J-W, Yustein JT, Lee

    LA, Dang CV: Myc stimulates nuclearly encoded mitochondrial genes and mitochondrial

    biogenesis. Mol Cell Biol [Internet] 2005, 25:6225–6234. Available from:

http://dx.doi.org/10.1128/MCB.25.14.6225-6234.2005

59. Koh CM, Bieberich CJ, Dang CV, Nelson WG, Yegnasubramanian S, De Marzo AM: MYC
    and Prostate Cancer. Genes Cancer [Internet] 2010, 1:617–628. Available from:
    http://dx.doi.org/10.1177/1947601910379132

60. Trabzonlu L, Kulac I, Zheng Q, Hicks JL, Haffner MC, Nelson WG, Sfanos KS, Ertunc O,
    Lotan TL, Heaphy CM, Meeker AK, Yegnasubramanian S, De Marzo AM: Molecular
    Pathology of High-Grade Prostatic Intraepithelial Neoplasia: Challenges and Opportunities.
    Cold Spring Harb Perspect Med [Internet] 2018, . Available from:
    http://dx.doi.org/10.1101/cshperspect.a030403

61. Rantanen A, Larsson NG: Regulation of mitochondrial DNA copy number during
    spermatogenesis. Hum Reprod [Internet] 2000, 15 Suppl 2:86–91. Available from:
    http://dx.doi.org/10.1093/humrep/15.suppl_2.86

62. Larsson NG, Oldfors A, Garman JD, Barsh GS, Clayton DA: Down-regulation of
    mitochondrial transcription factor A during spermatogenesis in humans. Hum Mol Genet
    [Internet] 1997, 6:185–191. Available from: http://dx.doi.org/10.1093/hmg/6.2.185

63. Choudhury D, Levi M: Kidney aging—inevitable or preventable? Nat Rev Nephrol [Internet]
    2011, 7:706–717. Available from: https://doi.org/10.1038/nrneph.2011.104

64. O'Sullivan ED, Hughes J, Ferenbach DA: Renal Aging: Causes and Consequences. J Am
    Soc Nephrol [Internet] 2017, 28:407–420. Available from:
    http://dx.doi.org/10.1681/ASN.2015121308

65. Wang XX, Takahashi S, Libby AE, Myakala K, Jones BA, Bhasin K, Qi Y, Krausz K, Zerfas

P, Panov J, Velenosi TJ, Patel DP, Daneshpajouhnejad P, Ginley B, Sarder P, Titievsky A, Sharov V, Ostretsov B, Kopp JB, Rosenberg AZ, Gonzalez FJ, Guha U, Brodsky L, Burris T, Levi M: ERR agonism reverses mitochondrial dysfunction and inflammation in the aging kidney [Internet]. bioRxiv. 2019 [cited 2019 Nov 7], p. 755801. Available from: https://www.biorxiv.org/content/10.1101/755801v1

66. Derényi I, Szöllősi GJ: Hierarchical tissue organization as a general mechanism to limit the accumulation of somatic mutations. Nat Commun [Internet] 2017, 8:14545. Available from: http://dx.doi.org/10.1038/ncomms14545

67. Bogenhagen D, Clayton DA: Mouse L cell mitochondrial DNA molecules are selected randomly for replication throughout the cell cycle. Cell [Internet] 1977, 11:719–727. Available from: http://dx.doi.org/10.1016/0092-8674(77)90286-0

68. Magnusson J, Orth M, Lestienne P, Taanman J-W: Replication of mitochondrial DNA occurs throughout the mitochondria of cultured human cells. Exp Cell Res [Internet] 2003, 289:133–142. Available from: http://dx.doi.org/10.1016/s0014-4827(03)00249-0

69. Trinei M, Berniakovich I, Pelicci PG, Giorgio M: Mitochondrial DNA copy number is regulated by cellular proliferation: A role for Ras and p66Shc. Biochimica et Biophysica Acta (BBA) - Bioenergetics [Internet], Elsevier, 2006, 1757:624–630. Available from: http://www.sciencedirect.com/science/article/pii/S0005272806001654

70. Muncan V, Sansom OJ, Tertoolen L, Phesse TJ, Begthel H, Sancho E, Cole AM, Gregorieff A, de Alboran IM, Clevers H, Clarke AR: Rapid loss of intestinal crypts upon conditional deletion of the Wnt/Tcf-4 target gene c-Myc. Mol Cell Biol [Internet] 2006, 26:8418–8426. Available from: http://dx.doi.org/10.1128/MCB.00821-06

71. Grayson AR, Walsh EM, Cameron MJ, Godec J, Ashworth T, Ambrose JM, Aserlind AB, Wang H, Evan G, Kluk MJ, Bradner JE, Aster JC, French CA: MYC, a downstream target of BRD-NUT, is necessary and sufficient for the blockade of differentiation in NUT midline carcinoma. Oncogene [Internet] 2014, 33:1736–1742. Available from: http://dx.doi.org/10.1038/onc.2013.126

72. Berger E, Rath E, Yuan D, Waldschmitt N, Khaloian S, Allgäuer M, Staszewski O, Lobner EM, Schöttl T, Giesbertz P, Coleman OI, Prinz M, Weber A, Gerhard M, Klingenspor M, Janssen K-P, Heikenwalder M, Haller D: Mitochondrial function controls intestinal epithelial stemness and proliferation. Nat Commun [Internet] 2016, 7:13171. Available from: http://dx.doi.org/10.1038/ncomms13171

73. Reznik E, Miller ML, Şenbabaoğlu Y, Riaz N, Sarungbam J, Tickoo SK, Al-Ahmadie HA, Lee W, Seshan VE, Hakimi AA, Sander C: Mitochondrial DNA copy number variation across human cancers. Elife [Internet] 2016, 5. Available from: http://dx.doi.org/10.7554/eLife.10769

74. Müller-Höcker J, Horvath R, Schäfer S, Hessel H, Müller-Felber W, Kühr J, Copeland WC, Seibel P: Mitochondrial DNA depletion and fatal infantile hepatic failure due to mutations in the mitochondrial polymerase γ (POLG) gene: a combined morphological/enzyme histochemical and immunocytochemical/biochemical and molecular genetic study. J Cell Mol Med [Internet] 2011, 15:445–456. Available from: http://dx.doi.org/10.1111/j.1582-4934.2009.00819.x

FIGURE LEGENDS

Figure 1. *In situ* assay specificity verified by DNase pretreatment. *MT-CO1* sense DNA *in situ* hybridization assay on FFPE prostate tissues without RNase A (**A**), with RNase A (**B**), without DNase I (**C**), and with DNase I (**D**) pretreatments. Original magnification x40.

Figure 2. Dose-dependent stepwise reduction in hybridization signals after forced reductions in mtDNA by 2′,3′-Dideoxycytidine (ddC) in (**A**) PC3 and (**B**) 22Rv1 prostate cancer cell lines. The cells were treated for 9 days, and fixed in 10% formalin and processed into paraffin blocks and sectioned. Original magnification x20.

Figure 3. Time-dependent reduction in mtDNA copy number measured by quantitative PCR in prostate cancer cell lines treated with ddC. ddC concentration: 3 uM for PC3, 30 uM for 22Rv1. **A**: Stepwise reduction in the ratio of mtDNA to nuclear DNA for two different primer/probe sets. **B**: The ratios of mtDNA/nuclear DNA content from these two sets of primer pairs were highly correlated. Relative standard curve method was used to calculate the quantity of each amplified product. Fold differences were determined by defining the ratio of mtDNA gene to nuclear DNA gene in day 0 cells as 1.0. All qPCR reactions including the standard curve were performed in triplicate. Data are represented as means ± SD.

Figure 4. Quantitative nature of the *in situ* assay for mtDNA copy number determined by strong positive correlation between qPCR and the area-fraction of mtDNA signals by image analysis. **A**: Stepwise decrease in mtDNA *in situ* signals in relation to duration of drug treatment in FFPE cell blocks. **B**: Example of Halo™ interface for image analysis. **C**: Correlations between relative mtDNA content by qPCR and by area-fraction using Halo™.

Figure 5. Cross section from the neck region from a 2-month-old female FVB/N female mouse.

A-F: Strong mtDNA signals were present in the basal compartment of squamous epithelium in the esophagus, as well as in skeletal muscle, and glandular tissues including the tracheal epithelium, submucosal glands and thyroid. Very low hybridization signals were seen in tracheal cartilage (**B**). Brown adipose tissue also showed very high levels of mtDNA signals (**E-F**).

Figure 6. Cross section of an adrenal gland from a 2-month-old female FVB/N mouse. The adrenal medulla showed much lower mtDNA signals than the cortex. The cortex showed variation in different zones with prominent *in situ* signal in the X-zone. Original magnification x10 (left), x40 (right).

Figure 7. Cross section of a kidney from a 2-month-old male FVB/N mouse. **A-B**: Very low hybridization signal levels were present in the glomeruli. Epithelial cells in distal convoluted tubules showed higher mtDNA signals than those in proximal tubules. **C-D**: Collecting ducts in medullary rays and in the medulla showed notably reduced mtDNA hybridization signals.

Figure 8. Cross section of liver from a 2-month-old male FVB/N mouse. There was a zonal distribution to mtDNA hybridization signals such that higher levels were present in the periportal hepatocytes and lower levels in the pericentral ones (**A**). **B** shows a higher magnification image of **A**.

Figure 9. *In situ* hybridization staining of mtDNA and telomeres on frozen human duodenum. **A**: Epithelial cells in the crypts and transit/amplifying cell compartments had higher mtDNA *in situ* signals than to those in the villus tips. **B**: Telomeric DNA *in situ* hybridization on adjacent slides of **A** as a control for probe penetrance. Strong telomeric DNA signals were seen through the bottom of the crypts to the top of the villus. **C** and **D** are higher magnification images of **A** and **B**, respectively. Original magnification x10 (**A** and **B**), x20 (**C** and **D**).

Figure 10. mtDNA *in situ* hybridization in kidneys from young, aging, and aging with calorie restriction C57BL/6 mice. In the aging mouse kidney, decreased mtDNA levels were identified in tubules, which was prevented by calorie restriction. n=3 for each group. Bottom panel is higher magnification images of top panel. Original magnification x10 (top panel), x40 (bottom panel).

SUPPLEMENTAL FIGURE LEGENDS

Figure S1. A reduction of the mtDNA encoded protein MT-CO1 accompanied the loss of mtDNA in a time-dependent manner in response to ddC treatment. The COX-IV protein remained present. Original magnification x40.

Figure S2. In human cancer cell xenografts, the mouse mtDNA probes only bound to the mouse stromal cells, and the human mtDNA probes only bound to human tumor cells.

Figure S3. Colocalization of MT-CO1 *in situ* signals (mtDNA) and MRPL12 protein. Note the puncta nature of mtDNA signals present exclusively in the cytoplasm.

Figure S4. Representative staining of mtDNA in the bladder of a 2-month-old female FVB/N mouse. High levels of mtDNA signals were present in umbrella cells compared to the underlying intermediate or basal epithelial cells. Original magnification x4 (left), x40 (right).

Figure S5. Representative staining of mtDNA in the normal uterine cervix. The cells in the basal compartment showed higher mtDNA signals than cells toward the surface.

Figure S6. Representative staining of mtDNA in different stages of hair growth cycle of mouse. Hair follicles in anagen growth phase (**A** and **B**) showed intense signals in the deepest regions with a gradation of signals towards the skin surface. Hair follicles in telogen phase had considerably lower mtDNA *in situ* signals (**C**). Mammary glands (inset in **C**) also stained with strong mtDNA *in situ* signals, similar to other glandular tissues. Original magnification x4 (**A** and **C**), x20 (**B**).

Figure S7. Representative staining of mtDNA in stomach from a 3-month-old male FVB/N mouse. The stem/proliferative cells in the isthmus showed higher mtDNA signals than the surface or deeper glands.

Figure S8. Representative staining of mtDNA in the normal human prostate. Basal cells contained increased mtDNA signals as compared to luminal cells. The stromal cells showed overall lower signals than the prostate epithelium.

Figure S9. Representative staining of mtDNA in the mouse male reproductive system. In the seminiferous tubules of the testis, strong signals were present in germ cells adjacent to the basement membrane, and signals decreased as cells differentiated towards mature sperm in the lumens. In the epididymis, there were more mtDNA signals in the tail epithelium than those in the head.

Figure S10. Representative staining of mtDNA in the mouse female reproductive and urinary system. The epithelium in mouse fallopian tube and uterus endometrium had strong mtDNA *in situ* signals. In the mouse ovary, in regions containing follicles, there were very strong signals in the granulosa cells directly surrounding the oocytes, with many, albeit less numerous, signals in the oocyte cytoplasm. Immature corpora lutea showed higher mtDNA signals compared to the mature corpora lutea.

Figure S11. Representative staining of mtDNA in the mouse cerebellum. Strong signals were observed in purkinje cell neuronal cell bodies and in neuronal cell bodies within a deep cerebellar nucleus.
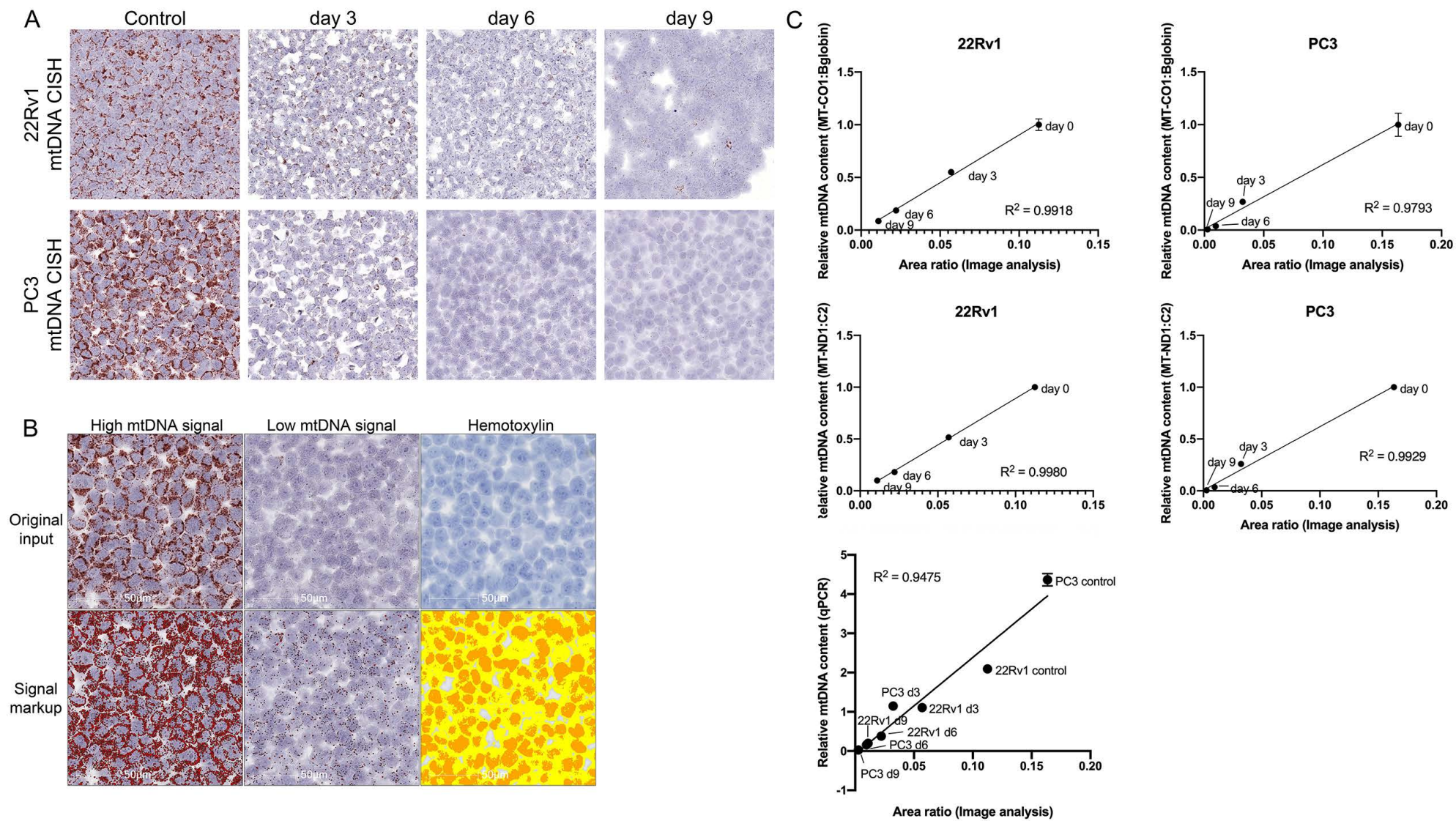
Figure 1

Figure 2

Figure 3

A

B
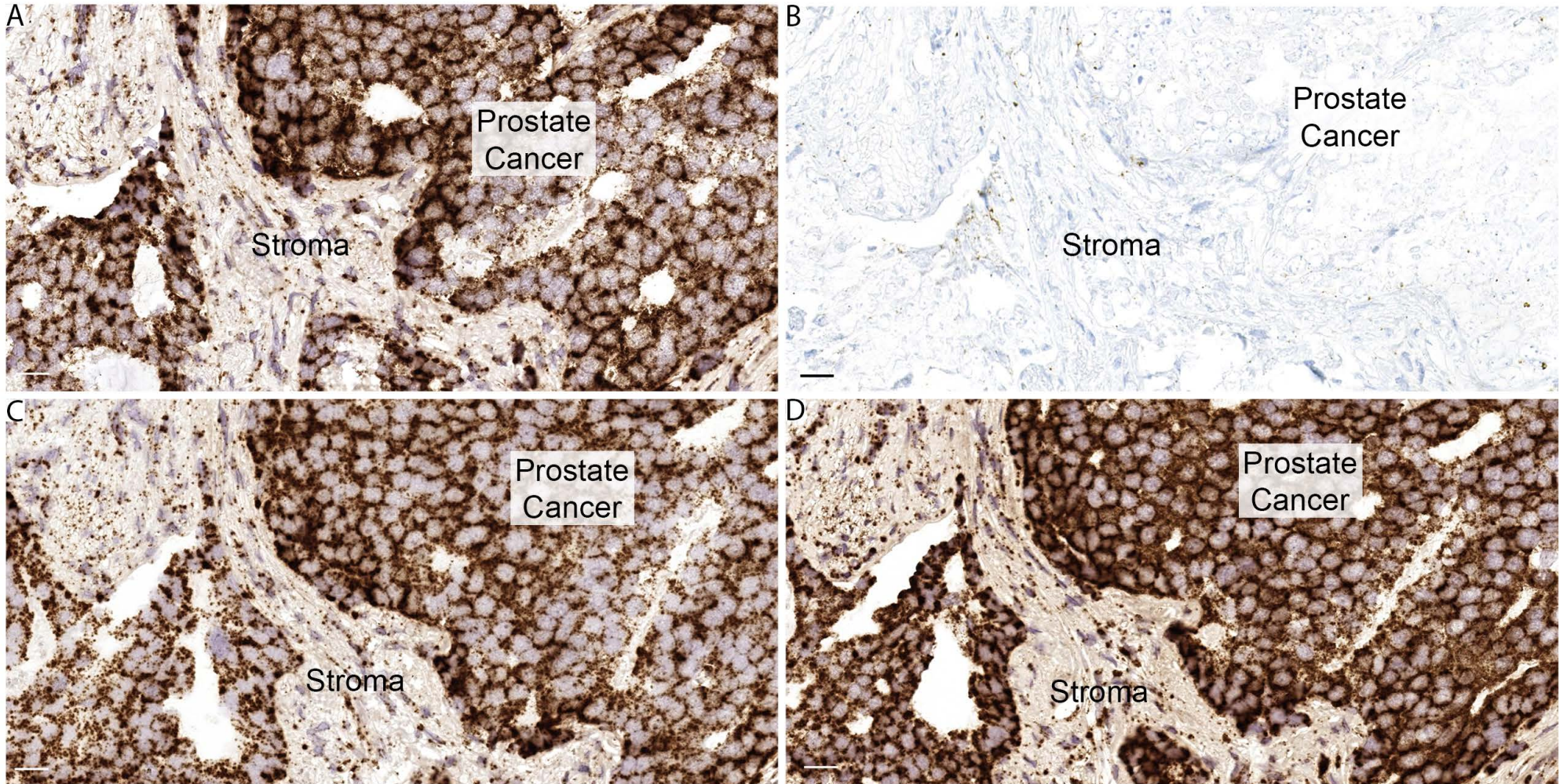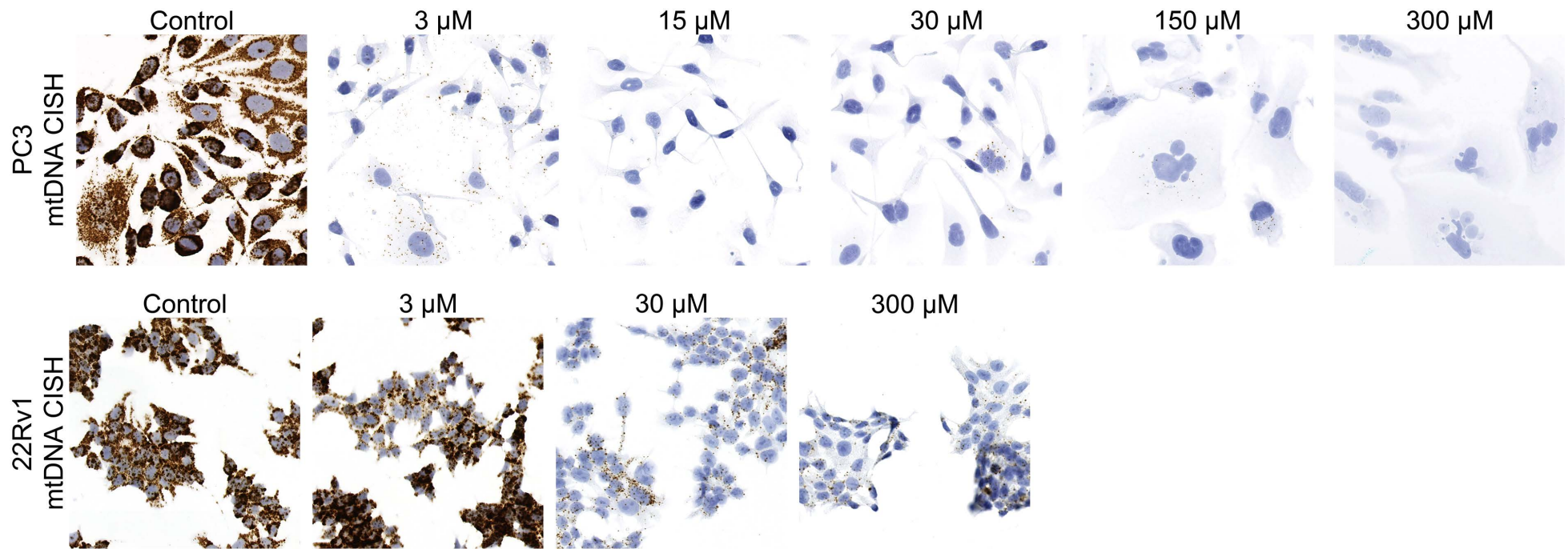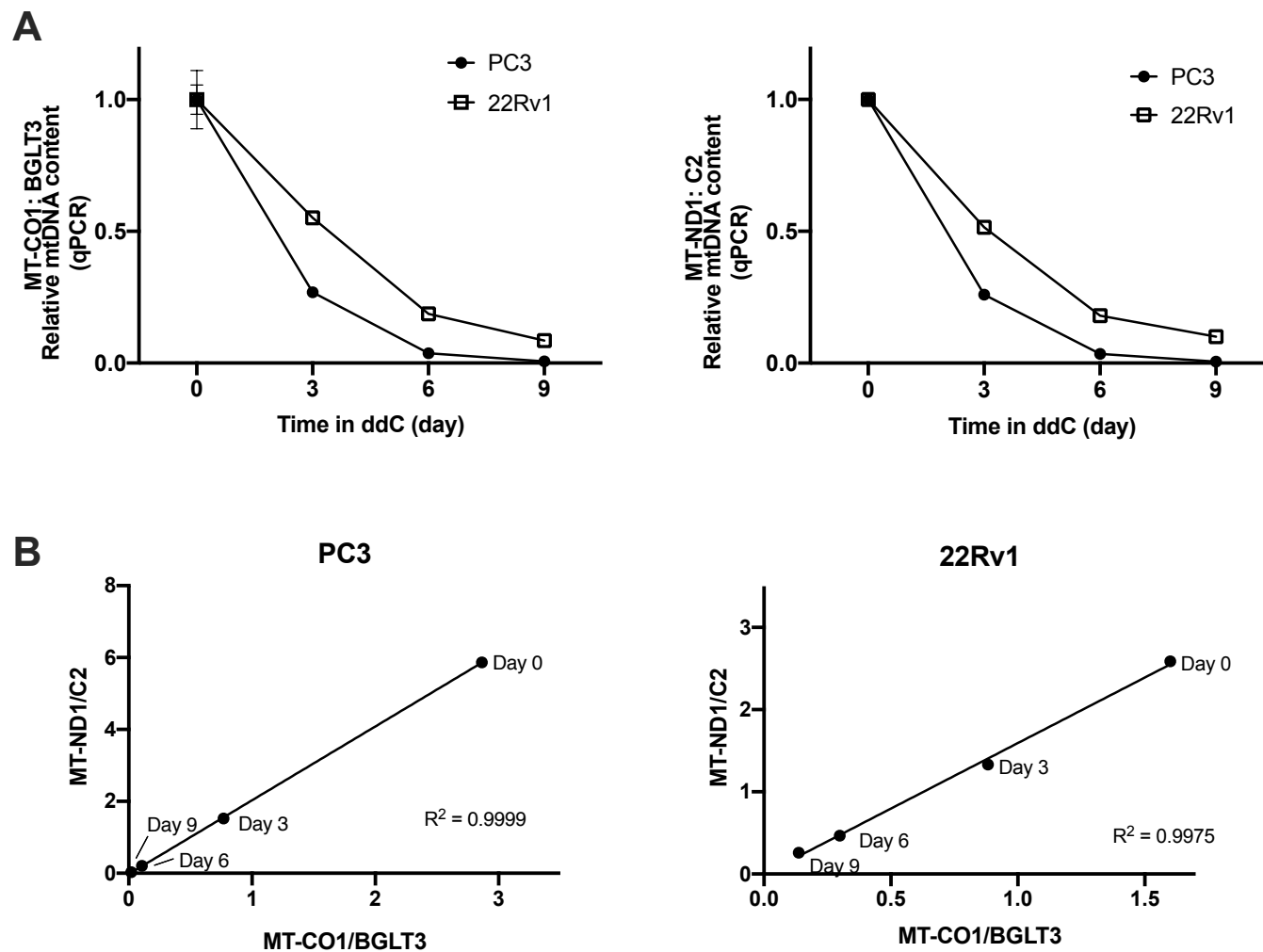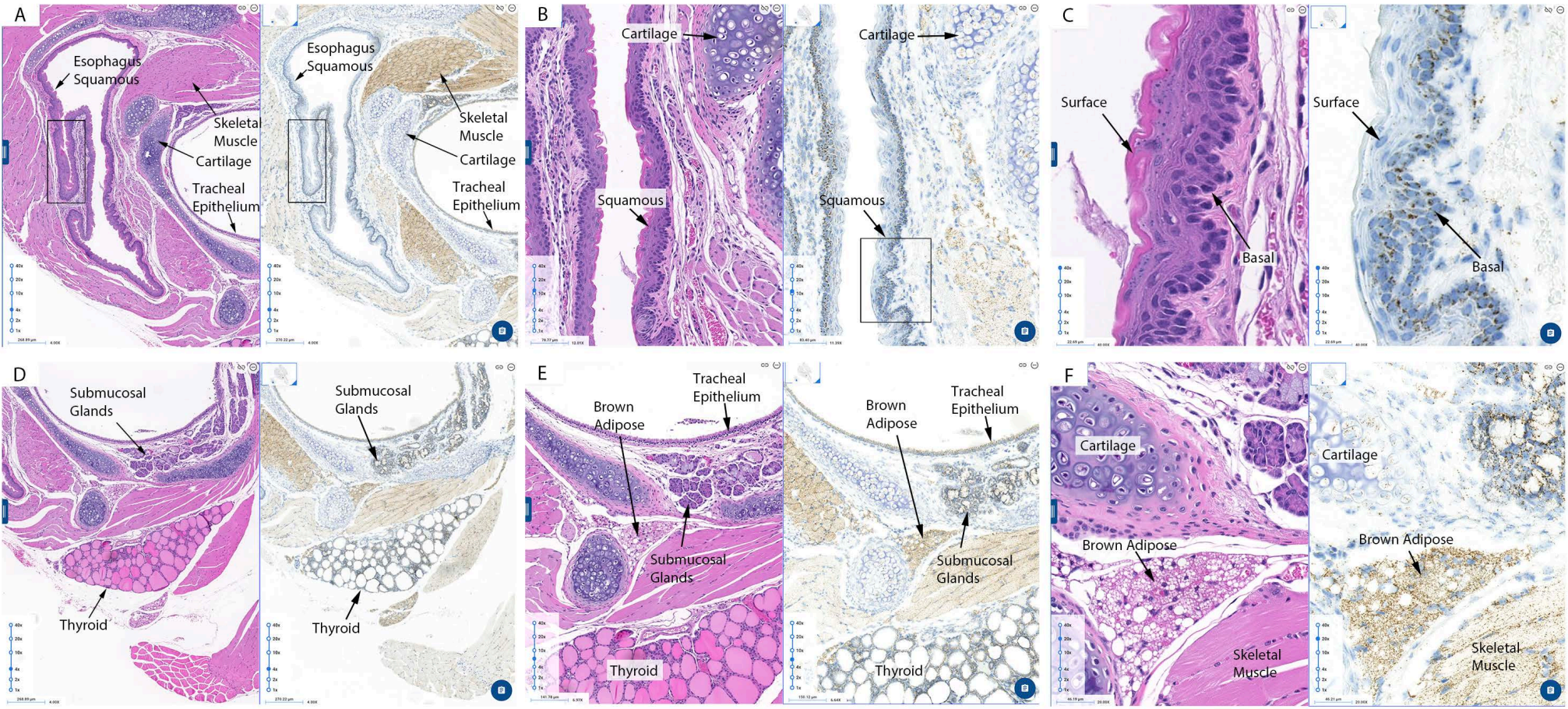
Figure 4

Figure 5

Figure 6

Figure 7

Figure 8

A: Portal Triads, Central Veins

B: Central Vein, Portal Area

Figure 9

A — mtDNA MT-CO1. Labels: Villus Tips, Transit Amplifying Cells, Crypts.
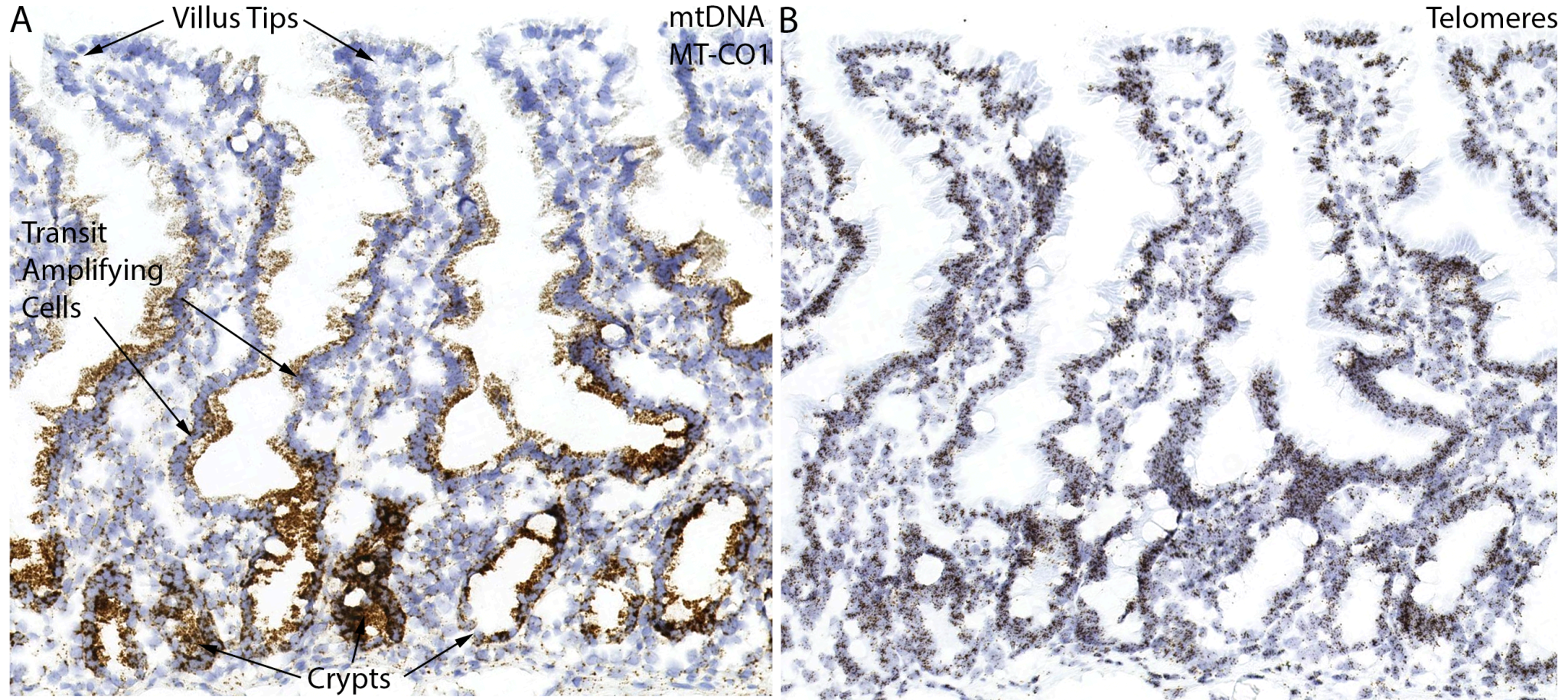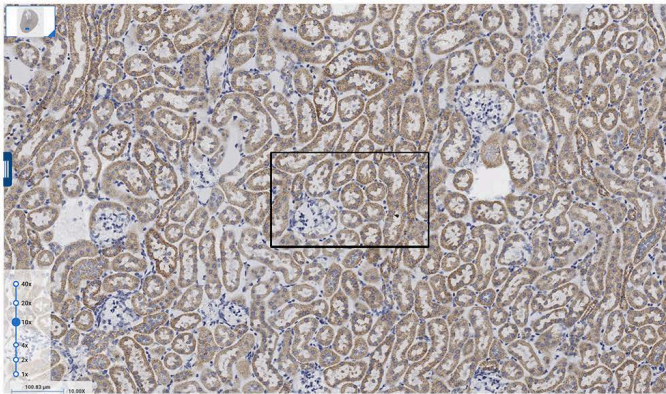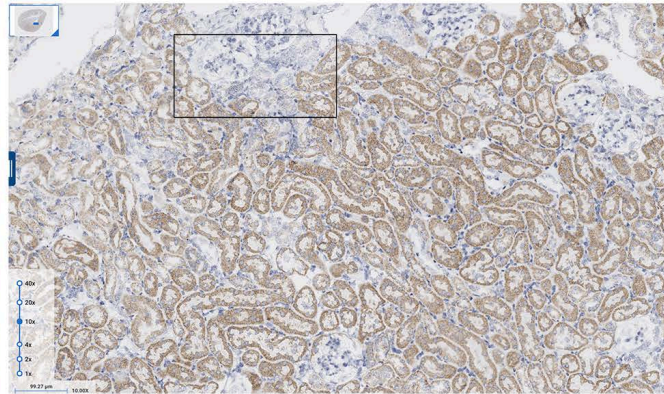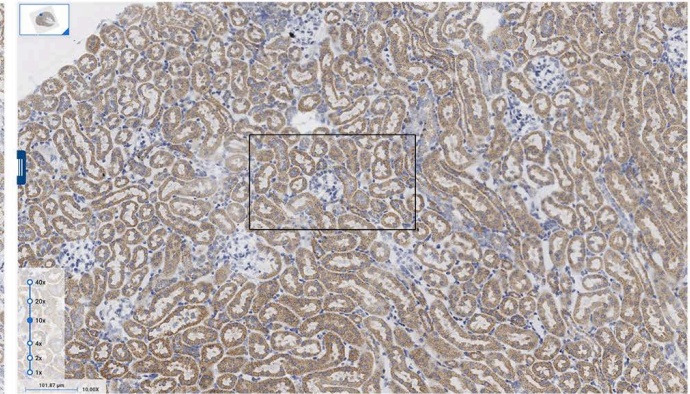
B — Telomeres.
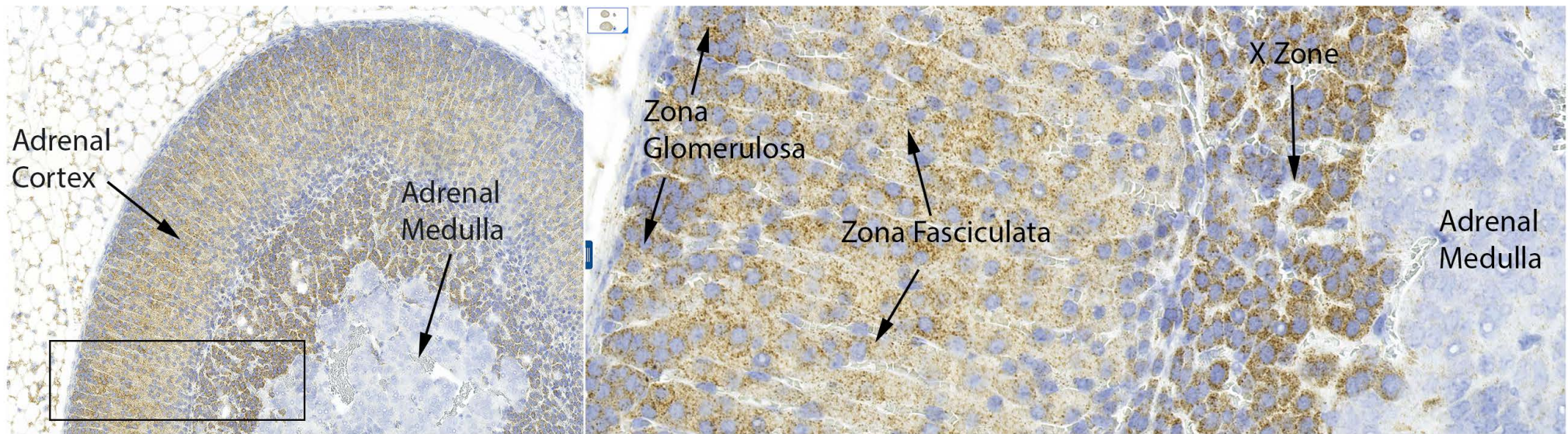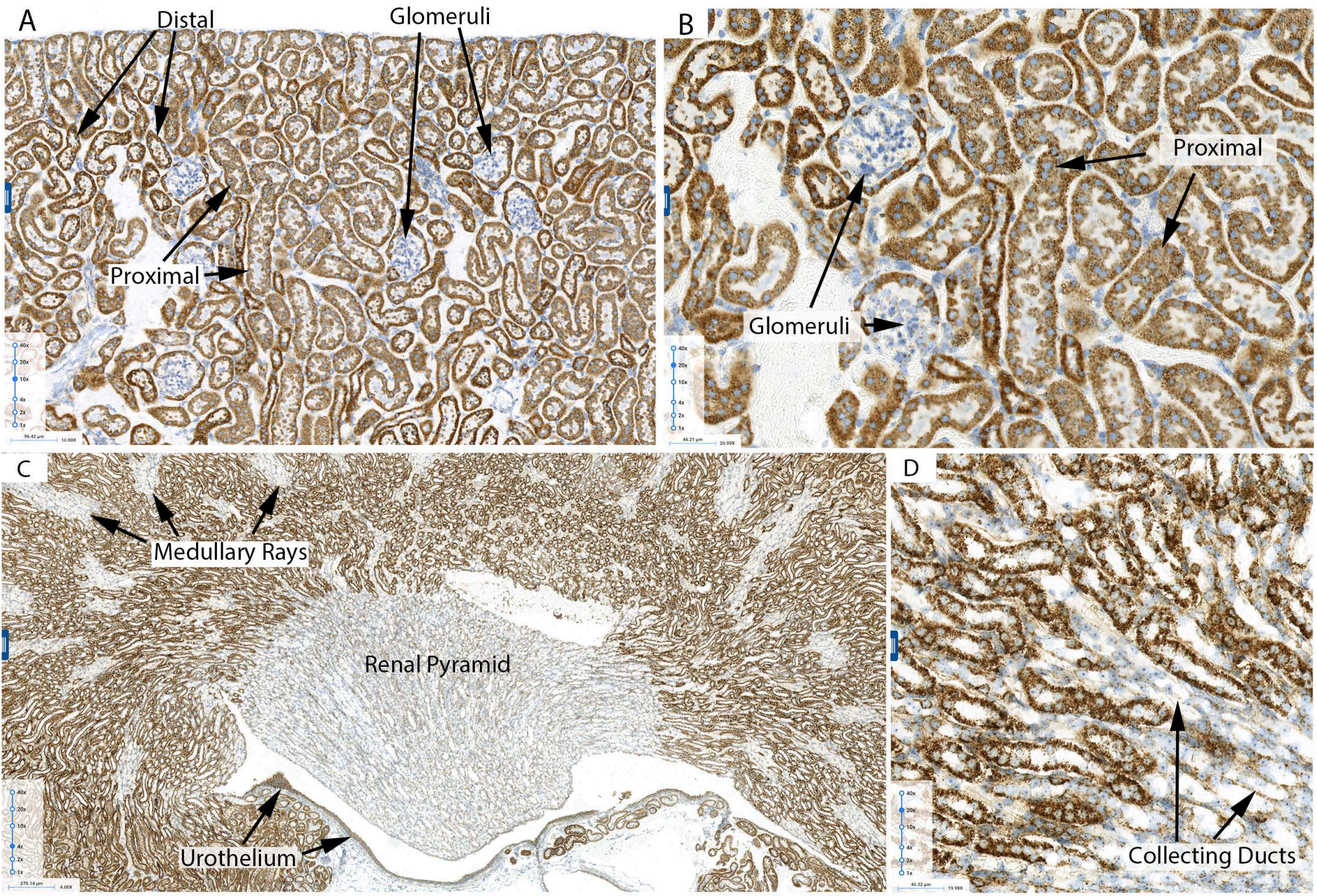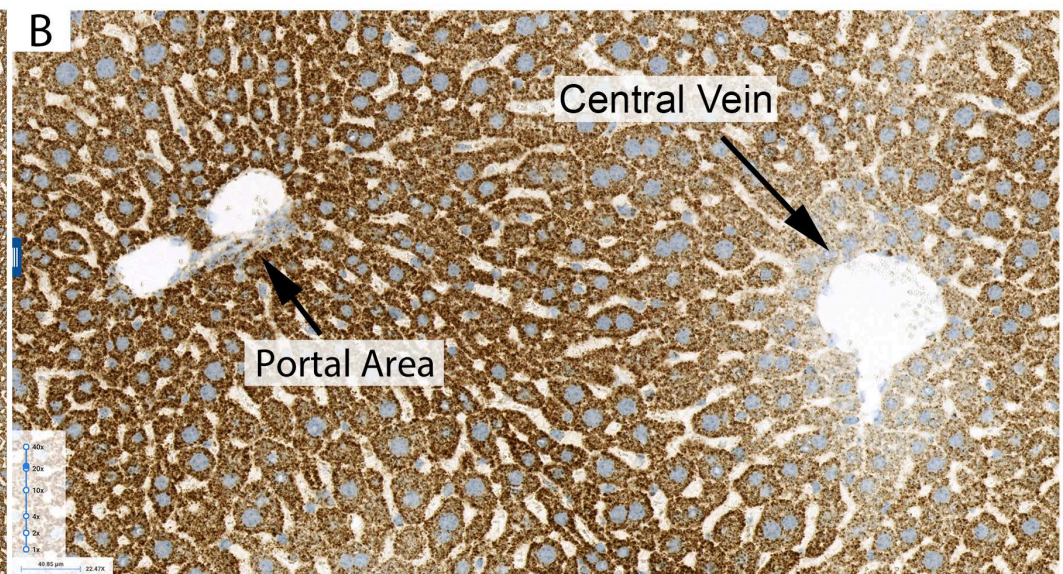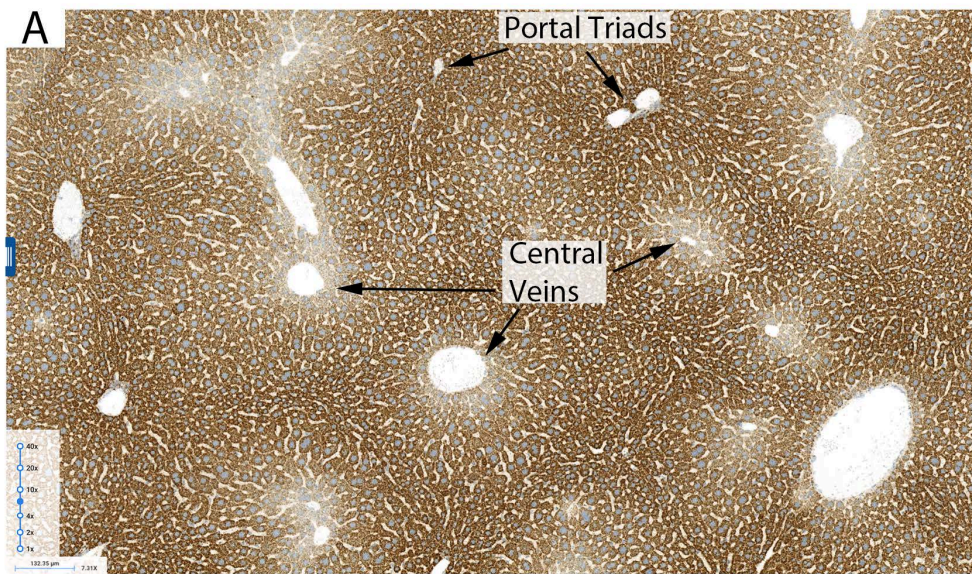
Figure 10

Young Mouse
Animal #1

Old Mouse
Animal #5

Old Mouse, Calorie Restricted
Animal #3